Ultrabroadband supercontinuum generation in a CMOS-compatible platform

R. Halir,[1,5,*] Y. Okawachi,[2] J. S. Levy,[3] M. A. Foster,[4] M. Lipson,[3,5] and A. L. Gaeta[2,5]

[1]*Departamento Ingeniería de Comunicaciones, ETSI Telecomunicación, Universidad de Málaga, 29010 Málaga, Spain*

[2]*School of Applied and Engineering Physics, Cornell University, Ithaca, New York 14853, USA*

[3]*School of Electrical and Computer Engineering, Cornell University, Ithaca, New York 14853, USA*

[4]*Department of Electrical and Computer Engineering, The Johns Hopkins University, Baltimore, Maryland 21218, USA*

[5]*Kavli Institute at Cornell for Nanoscale Science, Cornell University, Ithaca, New York 14853, USA*

**Corresponding author: robert.halir@ic.uma.es*

Received January 30, 2012; revised March 1, 2012; accepted March 13, 2012;
posted March 14, 2012 (Doc. ID 162267); published May 10, 2012

We demonstrate supercontinuum generation spanning 1.6 octaves in silicon nitride waveguides. Using a 4.3 cm-long waveguide, with an effective nonlinearity of $\gamma = 1.2\ \mathrm{W^{-1}\,m^{-1}}$, we generate a spectrum extending from 665 nm to 2025 nm (at –30 dB) with 160 pJ pulses. Our results offer potential for a robust, integrated, and low-cost supercontinuum source for applications including frequency metrology, optical coherence tomography, confocal microscopy, and optical communications.

OCIS codes: 190.4390, 320.7110, 320.6629, 230.7370.

Supercontinuum generation (SCG) in photonic crystal fibers, as first demonstrated in [1], has enabled key advances in spectroscopy [2], optical coherence tomography [3], pulse compression [4], and frequency metrology [5]. In particular, generation of an octave-spanning supercontinuum is crucial for the self-stabilization of optical frequency combs using f-to-$2f$ interferometry, which enables precision measurement of absolute optical frequencies [6]. While microstructured fibers continue to be efficient for SCG [7–9], the use of an integrated photonics chip for this purpose is attracting significant attention since it provides the first step towards integrated solutions and has the potential for high-volume, low-cost fabrication, especially if the platform is complementary metal-oxide-semiconductor (CMOS) compatible. Several materials have been proposed for integrated SCG. Chalcogenide waveguides exhibit a large effective nonlinearity ($\gamma \sim 10\ \mathrm{W^{-1}\,m^{-1}}$) and low two-photon absorption (TPA), and supercontinuum spanning up to 750 nm has been obtained with this material [10]. Recently, a 2.75 octave-spanning supercontinuum generated in periodically poled waveguides in lithium niobate has been reported [11]. However, neither material is easily incorporated into a CMOS process.

Silicon wire waveguides are fully CMOS compatible and exhibit large effective nonlinearities $\gamma \sim 10^2\ \mathrm{W^{-1}\,m^{-1}}$, due to their strong confinement and large nonlinear refractive index. While TPA generally limits the extent of SCG in silicon [12], by working near or below the half band gap of silicon (i.e., 2 μm), a 0.74 octave-spanning supercontinuum has been generated with such waveguides [13]. Alternatively, the use of CMOS-compatible high index glass with an effective nonlinearity of $\gamma \sim 1.2\ \mathrm{W^{-1}\,m^{-1}}$ has been proposed in [14], where a supercontinuum spectrum exceeding 350 nm is reported. However, due to the relatively small nonlinearity, a 45 cm-long waveguide is required.

Here, we demonstrate SCG in integrated silicon nitride waveguides at a pump wavelength of 1.3 μm. These waveguides exhibit an effective nonlinearity of $\gamma \sim 1\ \mathrm{W^{-1}\,m^{-1}}$, are robust and CMOS compatible, and do not suffer from TPA [15]. Using dispersion engineered waveguides, we observe a supercontinuum spanning 1.6 octaves, from 665 nm to 2025 nm, which is, to the best of our knowledge, the broadest supercontinuum generated on a CMOS-compatible chip. This constitutes a significant step towards fully integrated supercontinuum sources, and owing to the octave-spanning bandwidth, shows promise for applications in frequency metrology, optical coherence tomography, confocal imaging, and optical communications.

SCG arises from the interplay of several nonlinear processes [16], and their generation is enhanced if the input pulse is launched near the zero group-velocity dispersion (GVD) point or in the anomalous GVD regime [10,14,16,17]. The former minimizes temporal pulse broadening, thereby preserving high peak powers and thus maintaining a strong nonlinear interaction. The latter regime enables soliton propagation, whose dynamics can contribute to spectral broadening [16,18].

The silicon nitride waveguides are fabricated using electron-beam lithography, as previously described [15]. In these waveguides, GVD due to the waveguide confinement can compensate the material GVD by adjusting the waveguide dimensions [19]. Figure 1 shows the dispersion of the fundamental TE mode for different waveguide widths. We use a 1100 nm wide waveguide and a pump wavelength of 1335 nm.

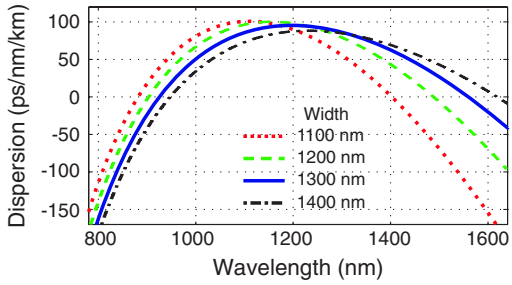

Fig. 1. (Color online) Simulated dispersion curves of the fundamental TE mode of a silicon nitride waveguide with a 720 nm height and widths ranging from 1100 nm to 1400 nm.

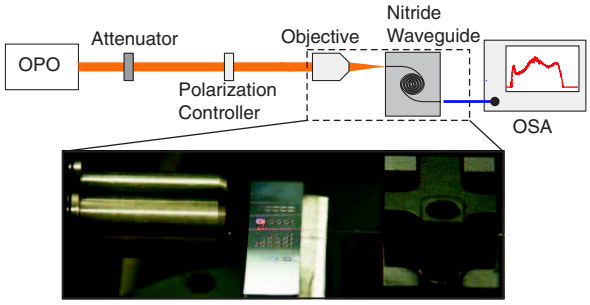

Fig. 2. (Color online) Setup for SCG with integrated silicon nitride waveguides. The enlarged section shows the coupling setup, in which part of the generated spectrum is visible as red radiation from the waveguide.

Figure 2 schematically shows the setup used in our experiments. An optical parametric oscillator (OPO) produces light pulses near 1300 nm with a duration of approximately 200 fs at a repetition rate of 80 MHz, which are free-space coupled into the chip using an aspheric lens. Neutral density filters are used to control the pulse energy, and the polarization is set to the quasi-TE (horizontal) state with a half-wave plate and a polarizer. The output from the waveguide is collected with a lensed fiber and sent to an optical spectrum analyzer (OSA). The coupling loss from the lens to the waveguide is –8.3 dB, and the waveguide propagation losses are measured to be 0.8 dB/cm. The silicon nitride waveguide used for SCG has an effective nonlinearity of $\gamma = 1.2\ \mathrm{W^{-1}\,m^{-1}}$ and a length of 4.3 cm.

To record the entire SCG spectrum, we utilize two OSAs with spectral ranges 600–1700 nm and 1200–2400 nm in combination with appropriate long-pass filters to avoid higher order diffraction effects. Figure 3 shows the experimental spectra we obtain for different pulse energies. At the lowest pulse energy (2.8 pJ), the spectrum experiences minimal broadening, and the shape of the input spectrum is preserved. The initial spectral broadening up to pulse energies of 19 pJ is mainly attributed to self-phase modulation (SPM). At 33 pJ, a prominent peak at 1800 nm appears, indicating dispersive wave generation. As the input pulse energy is further increased, we observe the feature shift to longer wavelengths (see line "B" in Fig. 3). A second distinct peak around 710 nm becomes visible with pulse energies of 58 pJ. This feature is spectrally narrow compared to the peak at 1800 nm, and, as indicated with line "A," does not experience frequency shifting. This second dispersive wave is visible to the eye as a red glow in the waveguide (see Fig. 2). As the power is further increased, the dispersive wave at the longer wavelength is further red-shifted, and the spectrum becomes flatter as a result of new intermediate frequency components being generated. At the maximum available pulse energy of 160 pJ, the supercontinuum extends over 1.6 octaves from 665 nm to 2025 nm at –30 dB, and over 1435 nm when measured from the noise level. Slight misalignment of the lensed fiber for output coupling at the highest pulse energy reduces the total measured power, but does not change the shape of the spectrum, thereby confirming that no spectral broadening is taking place inside the collection fiber. While this generated spectrum is not completely flat, the wavelength regimes about the

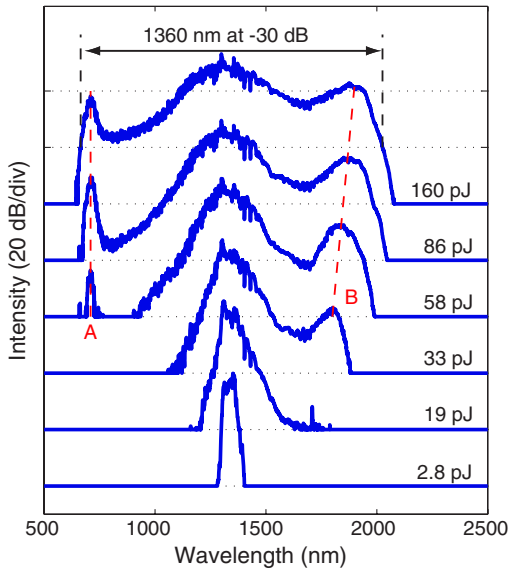

Fig. 3. (Color online) Measured spectra at the silicon nitride chip output. The spectra are progressively offset by 20 dB, and the pulse energy in the waveguide is indicated on the right side of each spectrum. Lines "A" and "B" highlight dispersive wave generation at short and long wavelengths, respectively.

710 nm and 1420 nm bands would be suitable for f-to-$2f$ interferometry.

We model the SCG using the generalized nonlinear envelope equation (GNEE) [20] including the effects of propagation loss, GVD to all orders, SPM, third-harmonic generation, and self-steepening. The contributions from the Raman effect are not included. These simulations are carried out using the silicon nitride waveguide characteristics with no free parameters. The spectral evolution of the generated supercontinuum as a function of input pulse energy is shown in Fig. 4. The simulated evolution predicts the short and long-wavelength dispersive features that are observed in the experimental spectra (labeled A and B in the figure). The circles in Fig. 4 indicate the experimentally measured peak wavelengths of the generated spectral features. The dashed lines show the predicted wavelength of phase-matching for the dispersive waves based on Eq. (2) from [21], including the increased peak power resulting from soliton-effect pulse compression prior to the dispersive wave genera-

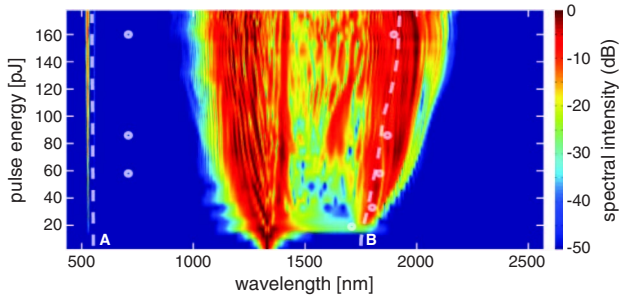

Fig. 4. (Color online) Simulated spectral evolution of the generated supercontinuum. The short and long-wavelength dispersive waves are labeled A and B, respectively. The dashed lines are the predicted wavelength of the dispersive waves based on a phase-matching analysis. The circles indicate the experimentally measured peak wavelength of the short and long-wavelength features.

tion [4]. Both the phase-matching analysis and the simulated spectral evolution accurately predict the position and shift of the long-wavelength spectral feature as a function of pulse energy. This indicates that the wavelength shift of the long-wavelength component is not due to the Raman soliton self-frequency shift. Furthermore, as observed experimentally, the short-wavelength feature is predicted to remain fixed spectrally; however, the predicted wavelength is bluer than that is measured. We attribute this inaccuracy to the uncertainty of the precise material dispersion of the deposited silicon nitride layer. Nevertheless, our modeling demonstrates that the observed spectral features and their dependence on pulse energy are well described by the dynamics of soliton-effect compression and dispersive wave generation within the silicon nitride waveguide.

In conclusion, we have experimentally demonstrated SCG spanning 1.6 octaves in silicon nitride waveguides with a pulse energy of 160 pJ. This constitutes, to the best of our knowledge, the broadest supercontinuum generated on a CMOS-compatible chip to date, with potential applications in frequency metrology, optical coherence tomography, confocal imaging, and optical communications. It furthermore demonstrates the potential of silicon nitride as a CMOS-compatible material for nonlinear optics, that, as opposed to silicon, does not suffer from the effects of TPA at communication wavelengths.

The authors would like to thank Matthew Graham, Henry Wen, and Pablo Londero for useful discussions. We acknowledge support from the Defense Advanced Research Projects Agency, the Center for Nanoscale Systems, supported by the National Science Foundation (NSF) and the New York State Foundation for Science, Technology, and Innovation, and FPU scholarship (AP-2006-03355) of the Spanish Ministerio de Ciencia e Innovación. This work was performed in part at the Cornell NanoScale Facility, a member of the National Nanotechnology Infrastructure Network, which is supported by the NSF (Grant ECS-0335765).

References

1. J. K. Ranka, R. S. Windeler, and A. J. Stentz, Opt. Lett. **25**, 25 (2000).
2. K. Lindfors, T. Kalkbrenner, P. Stoller, and V. Sandoghdar, Phys. Rev. Lett. **93**, 037401 (2004).
3. W. Drexler, J. Biomed. Opt. **9**, 47 (2004).
4. M. Foster, A. Gaeta, Q. Cao, and R. Trebino, Opt. Express **13**, 6848 (2005).
5. T. Udem, J. Reichert, R. Holzwarth, and T. Hänsch, Opt. Lett. **24**, 881 (1999).
6. D. Jones, S. Diddams, J. Ranka, A. Stentz, R. Windeler, J. Hall, and S. Cundiff, Science **288**, 635 (2000).
7. M. A. Foster and A. L. Gaeta, Opt. Express **12**, 3137 (2004).
8. G. Qin, X. Yan, C. Kito, M. Liao, C. Chaudhari, T. Suzuki, and Y. Ohishi, Appl. Phys. Lett. **95**, 161103 (2009).
9. A. M. Heidt, A. Hartung, G. W. Bosman, P. Krok, E. G. Rohwer, H. Schwoerer, and H. Bartelt, Opt. Express **19**, 3775 (2011).
10. M. R. Lamont, B. Luther-Davies, D.-Y. Choi, S. Madden, and B. J. Eggleton, Opt. Express **16**, 14938(2008).
11. C. Phillips, J. Jiang, C. Langrock, M. M. Fejer, and M. E. Fermann, Opt. Lett. **36**, 3912 (2011).
12. P. Koonath, D. R. Solli, and B. Jalali, Appl. Phys. Lett. **93**, 091114 (2008).
13. B. Kuyken, X. Liu, R. M. Osgood, Y. A. Vlasov, R. Baets, G. Roelkens, and W. M. Green, Opt. Express **19**, 20172 (2011).
14. D. Duchesne, M. Peccianti, M. R. Lamont, M. Ferrera, L. Razzari, F. Légaré, R. Morandotti, S. Chu, B. E. Little, and D. J. Moss, Opt. Express **18**, 923 (2010).
15. J. S. Levy, A. Gondarenko, M. A. Foster, A. C. Turner-Foster, A. L. Gaeta, and M. Lipson, Nature Photonics **4**, 37 (2009).
16. J. M. Dudley, G. Genty, and S. Coen, Rev. Mod. Phys. **78**, 1135 (2006).
17. I.-W. Hsieh, X. Chen, X. Liu, J. I. Dadap, N. C. Panoiu, C.-Y. Chou, F. Xia, W. M. Green, Y. A. Vlasov, and R. M. Osgood, Opt. Express **15**, 15242 (2007).
18. J. Herrmann, U. Griebner, N. Zhavoronkov, A. Husakou, D. Nickel, J. Knight, W. Wadsworth, P. Russell, and G. Korn, Phys. Rev. Lett. **88**, 173901 (2002).
19. A. C. Turner, C. Manolatou, B. S. Schmidt, M. Lipson, M. A. Foster, J. E. Sharping, and A. L. Gaeta, Opt. Express **14**, 4357 (2006).
20. G. Genty, P. Kinsler, B. Kibler, and J. M. Dudley, Opt. Express **15**, 5382 (2007).
21. M. A. Foster, A. C. Turner, M. Lipson, and A. L. Gaeta, Opt. Express **16**, 1300 (2008).